Electronic Supplementary Material (ESI) for Physical Chemistry Chemical Physics.

Supporting Information for: **5D Total Scattering Computed Tomography Reveals the Full Reaction Mechanism of a bismuth vanadate lithium ion battery anode**

Jonas Sottmann, Amund Ruud, Øystein S. Fjellvåg, Gavin B.M. Vaughan, Marco Di Michel, Helmer Fjellvåg, Oleg I. Lebedev, Poniah Vajeeston and David S Wragg

TSCT mapping

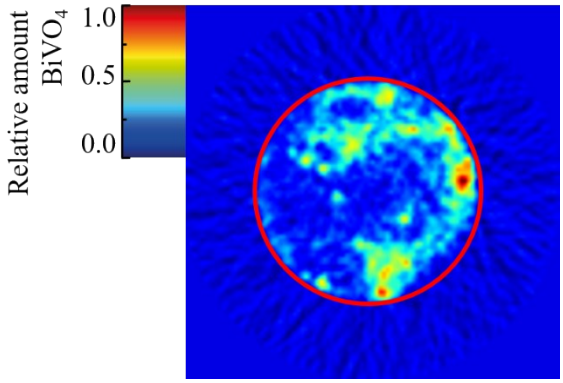

[Figure S1]. XRDCT map of the initial distribution of $BiVO_4$ used to mask out areas with no active material. The red circle marks the interface between the electrode and the cell casing. Beyond the circle, one can vaguely make out the signal from the glass walls.

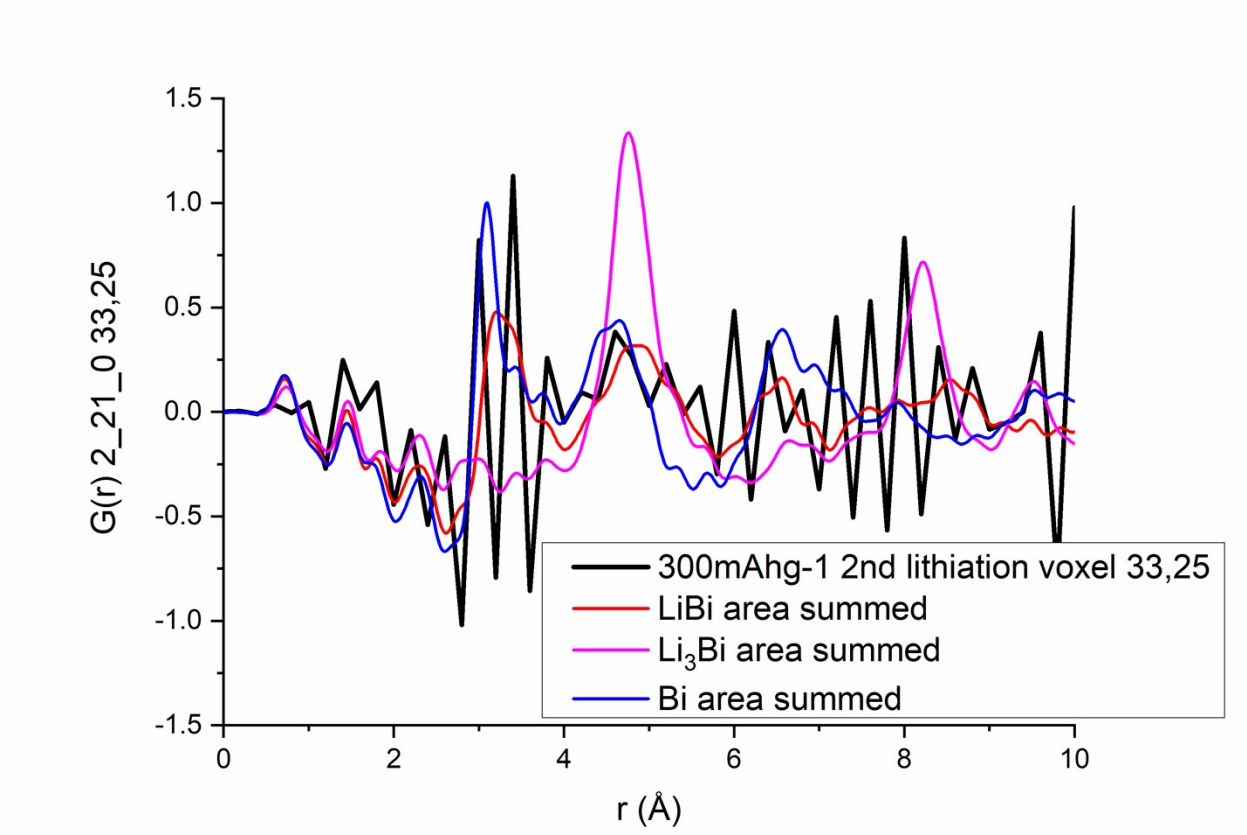

[Figure S2] comparison of the area summed PDFs for time points when Bi, LiBi and Li_3Bi were the dominant component, with 0.02 Å binning in r, and the PDF from a single voxel at 300mAg-1 capacity in the 2nd lithiation, with 0.2 Å binning in r.

Electrochemical results

To test long term stability a BiVO4 anode prepared as for the TSCT experiment was tested in a coin cell as a half cell against lithium metal for 500 cycles.

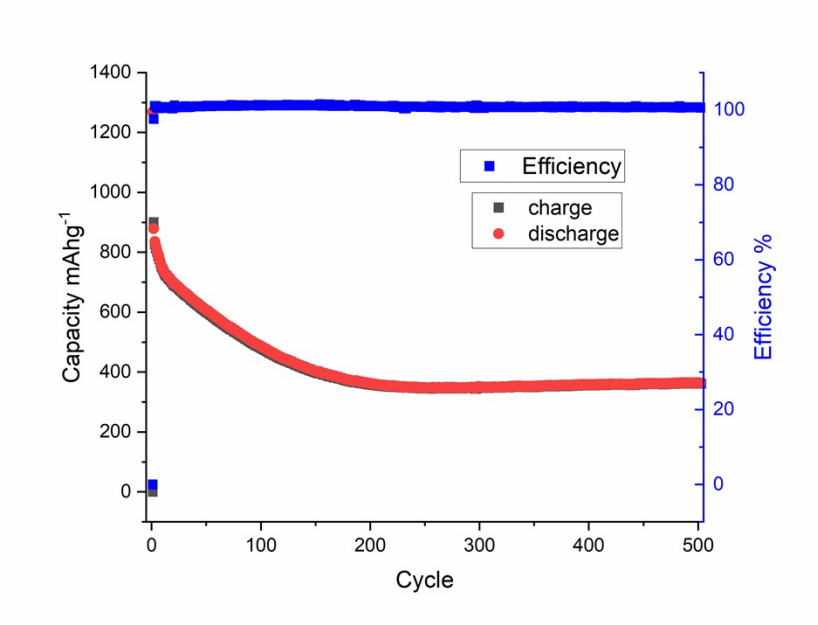

[Figure S3] Capacity and Coulombic efficiency plot for 500 cycles with a bismuth vanadate lithium ion half-cell. The first cycle was performed at a current density of 50 mA/g, subsequent cycles at 150 mA/g. The first discharge took ~24 hours (from 2.5 to 0.01 V), 1st charge ~17 hours, 2nd discharge ~6 h.

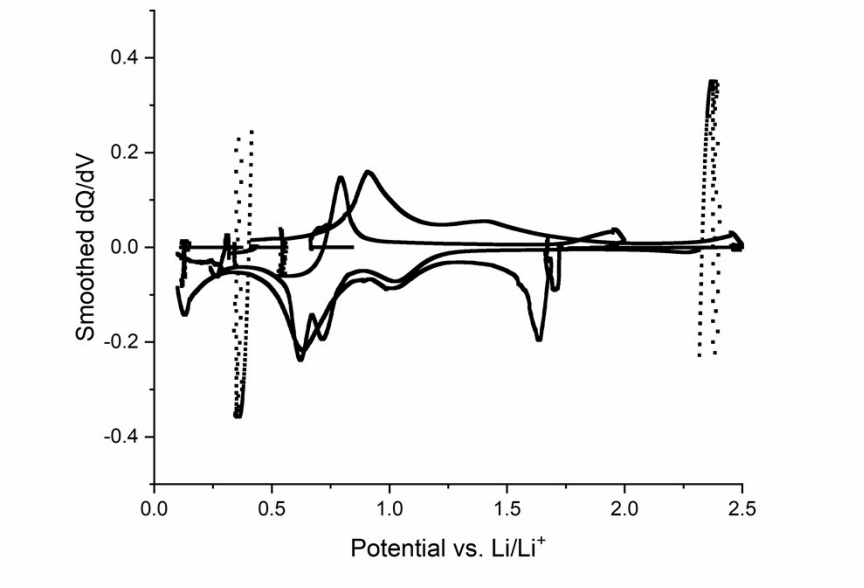

[Figure S4] dQ/dV curves calculated from the galvanostatic cycling data collected during the operando PDFCT experiment. The main features of the curve agree well with data from coin cells published elsewhere.[1]

PDF and Rietveld Fitting

PDF and Rietveld fitting was carried out in TOPAS V6[2] using a surface refinement approach,[3] meaning that groups datasets were refined simultaneously with some parameters refined separately for each

individual pattern/PDF (e.g. lattice parameters, crystallite size) and others refined against the all of the patterns together (e.g. zero point, thermal parameters at constant temperature). Attempts were made to refine the Rietveld and PDF data together using the same structural parameters, but were not successful. Because of the complex array of structures (some quite similar to one another) used to fit the data we were not able to use the same input file throughout the whole process as in several other fitting studies. Once we had established which phases were present at particular stages of cycling the input files were modified to exclude phases we were certain were not present (E.g. $BiVO_4$ after initial decomposition).

The model for the Bi clusters was obtained by clipping out atoms from the symmetry extended crystal structure of Bi metal and placing the resulting clusters in the middle of a cubic unit cell with no internal symmetry. The lattice parameters of the cell and the atom positions in the 8 atom cluster were manually adjusted until a reasonable fit was obtained. The resulting cluster was turned into a rigid body described by a Fensky-Hall Z-matrix in which the Bi-Bi bond lengths and angles could be refined within certain limits, with starting values being generated randomly. The unit cell edges were fixed to 20 Å in the final refinements. A spherical damping parameter was refined for each individual PDF. The Bi cluster part of the input file is shown below:

```
str

                pdf_zero -0.01

                phase_name "Bi_clust"

                space_group "P1"


                a !a_octo_1  20 min 8 max 25 val_on_continue = Rand(11,13);

                b =Get(a);

                c =Get(a);

                prm    r2_1  3.27904`_LIMIT_MIN_3                min 3.0   max 3.5  val_on_continue =
Rand(3,3.3);

                prm    r1_1  3.60000`_LIMIT_MIN_3                        min 3.0   max 3.6
        val_on_continue = Rand(3.3,3.6);

                prm    r3_1  3.08265`_LIMIT_MIN_3                min 3.0    max 3.5  val_on_continue =
Rand(3,3.3);

                prm    r4_1  3.00000`_LIMIT_MIN_3                min 3.0    max 3.5  val_on_continue =
Rand(3,3.3);

                prm    r5_1  3.00000`_LIMIT_MIN_3                min 3.0    max 3.5  val_on_continue =
Rand(3,3.3);

                prm    r6_1  3.60000`              min 3.0    max 3.6  val_on_continue = Rand(3.3,3.6);
```

prm r6_1 3.60000`_LIMIT_MIN_3 min 3.0 max 3.6 val_on_continue = Rand(3.3,3.6);

prm r7_1 3.60000`_LIMIT_MIN_3 min 3.0 max 3.6 val_on_continue = Rand(3.3,3.6);

prm bi3bi2_angle_1 90.90257`_LIMIT_MIN_85 min 85 max 95 val_on_continue = Rand(85,95);

prm bi4bi3_angle_1 90.00343`_LIMIT_MIN_85 min 85 max 95 val_on_continue = Rand(85,95);

prm bi4bi2_angle_1 74.90895` min 72 max 82 val_on_continue = Rand(72,82);

prm bi5bi4_angle_1 79.31196`_LIMIT_MIN_72 min 72 max 82 val_on_continue = Rand(72,82);

prm bi5bi3_angle_1 161.99113`_LIMIT_MIN_150 min 150 max 175 val_on_continue = Rand(150,175);

prm bi6bi5_angle_1 85.00000`_LIMIT_MIN_85 min 85 max 95 val_on_continue = Rand(85,95);

prm bi6bi4_angle_1 280.00000`_LIMIT_MIN_260 min 260 max 280 val_on_continue = Rand(260,280);

prm bi7bi6_angle_1 114.99999`_LIMIT_MIN_90 min 90 max 115 val_on_continue = Rand(90,115);

prm bi7bi5_angle_1 89.02245` min 85 max 95 val_on_continue = Rand(85,95);

prm bi8bi6_angle_1 170.61418`_LIMIT_MIN_170 min 170 max 190 val_on_continue = Rand(170, 190);

prm bi8bi5_angle_1 95.00000`_LIMIT_MIN_85 min 85 max 95 val_on_continue = Rand(89, 91);

rigid

z_matrix Bi1

z_matrix Bi2 Bi1 = r1_1; 'axial

z_matrix Bi3 Bi1 = r2_1; Bi2 = bi3bi2_angle_1;

z_matrix Bi4 Bi1 = r3_1; Bi3 = bi4bi3_angle_1; Bi2 = bi4bi3_angle_1;

z_matrix Bi5 Bi1 = r4_1; Bi4 = bi5bi4_angle_1; Bi3 = bi5bi3_angle_1;

```
z_matrix Bi6 Bi1 = r5_1; Bi5 = bi6bi5_angle_1;   Bi4  = bi6bi4_angle_1; 'axial
z_matrix Bi7 Bi1 = r6_1; Bi6 = bi7bi6_angle_1;   Bi5  = bi7bi6_angle_1;
z_matrix Bi8 Bi6 = r7_1; Bi1 = bi8bi6_angle_1;           Bi5 = bi8bi5_angle_1;


    translate
            tx  =Get(a)/2; :  10.00000
            ty  =Get(b)/2; :  10.00000
            tz  =Get(c)/2; :  10.00000
            operate_on_points "Bi1 Bi2 Bi3 Bi4 Bi5 Bi6 Bi7 Bi8"

            site Bi1   x  0.50000` y  0.50000` z  0.50000` occ Bi 1      max 1   beq  !BBi  1.3
            site Bi2   x  0.50000` y  0.50000` z  0.68000` occ Bi 1      max 1   beq  !BBi  1.3
'layer 2
            site Bi3   x  0.33607` y  0.50000` z  0.49742` occ Bi 0      max 1   beq  !BBi  1.3
            site Bi4   x  0.50001` y  0.34587` z  0.49999` occ Bi 1      max 1   beq  !BBi  1.3
'layer 3
            site Bi5   x  0.63944` y  0.47219` z  0.54777` occ Bi 1      max 1   beq  !BBi  1.3
    'layer 3
            site Bi6   x  0.55530` y  0.47209` z  0.36339` occ Bi 1      max 1   beq  !BBi  1.3
'layer2
            site Bi7          x  0.44370` y  0.66895` z  0.52622`       occ Bi 1 max 1   beq
!BBi  1.3
            site Bi8          x  0.61176` y  0.41118` z  0.20370`       occ Bi   1.00000 max 1
    beq  !BBi  1.3

            weight_percent wp_PDF_Bi_rom_nano_1  91.223`
            spherical_damping(r_Binano_1, 9.89846`_LIMIT_MIN_2 min 2 max 20)
            scale  scale_pdf_bi_clust_1  0.0940229599`_LIMIT_MIN_1e-015
```

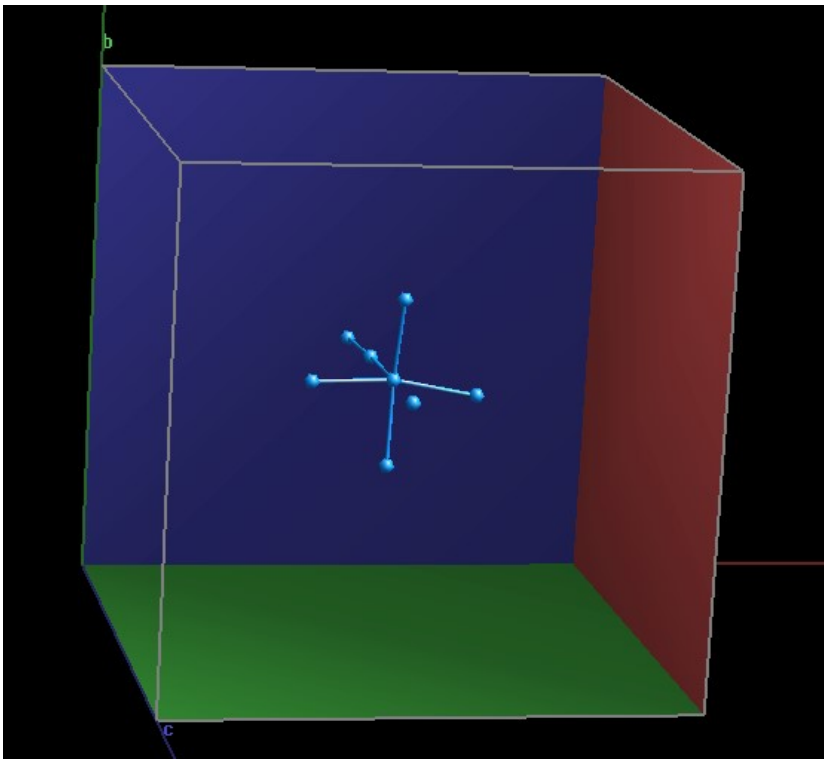

[Figure S5] The bismuth cluster used for PDF fitting of the amorphous data.

The PDF fitting of the other phases used the normal crystal structure models with spherical damping parameters applied to limit the radial extent of the PDF. Lattice parameters, spherical damping, scale factor and Bi thermal parameters were refined for all phases except the nanosized Li3Bi which required a fixed spherical damping for stable refinement.

The Rietveld fits, from the point where Bragg peaks reappear (around 350 $mAhg^{-1}$) in the delithiation onwards, used the same models for Bi, LiBi and Li_3Bi. Only the 3 crystalline phases were refined and the amorphous phases were treated as background. The background was fitted with a 3-term Chebyshev polynomial, a scaled background measurement from an empty capillary and a Pawley phase based on the Bi metal unit cell to fit other broad background features (max Lorentzian crystallite size for fundamental parameters (FP) broadening limited to 2 nm). All 3 phases could be refined against all patterns containing Bragg peaks and it was not necessary to remove phases at certain stages (the relevant scales refined to approximately zero when phases were not present). Fixed thermal parameters were used throughout. Lattice parameters, scales and FP crystallite size were refined for all the phases. Initial line width for the FP model was obtained by fitting the CeO_2 detector calibration pattern. Examples of the fits obtained [esi_fits] and a plot of Rwp [rwp_support] are shown below.

Fitting of V-O and C-C PDF peaks

V-O and C-C bond lengths PDF peaks were fitted in TOPAS V6 using a simple peak fit with no theta dependence over the range r = 1.15 to 2.55 Å. 3 xo_Is type pseudo-Voigt peaks were refined. An excerpt of the inp file is provided below:

lam no_th_dependence la 1 lo 0 lh 1

bkg @ -0.770296821`_0.0996016513 -0.0689624134`_0.0349358749 0.190625482`_0.0296233709

start_X 1.15 'Removes lower r values from future calculations

finish_X 2.55 'Removes higher r values from future calculations

xo_ls

local c1 1.43944`_0.00211 min 1.3 max 1.6

local c2 2.32042`_0.00382 min 2.0 max 2.5

local vo1 1.78992`_0.00582 min 1.7 max 1.9

xo =c1;:1.43944`_0.00211139731 I @  0.33003`_0.06005

xo =vo1;: 1.78992`_0.00581538342 I @  0.29588`_0.06602

xo =c2;: 2.32042`_0.00381893317 I @  0.62417`_0.11068

PV_Peak_Type(@, 0.17017`_0.03576,@, 3.61986`_4.08942,@, 0.17012`_0.03572,@, 0.87750`_0.01943_LIMIT_MIN_0.0001,@, 0.30500`_0.01943_LIMIT_MIN_0.0001,@, 0.30500`_0.01943_LIMIT_MIN_0.0001)

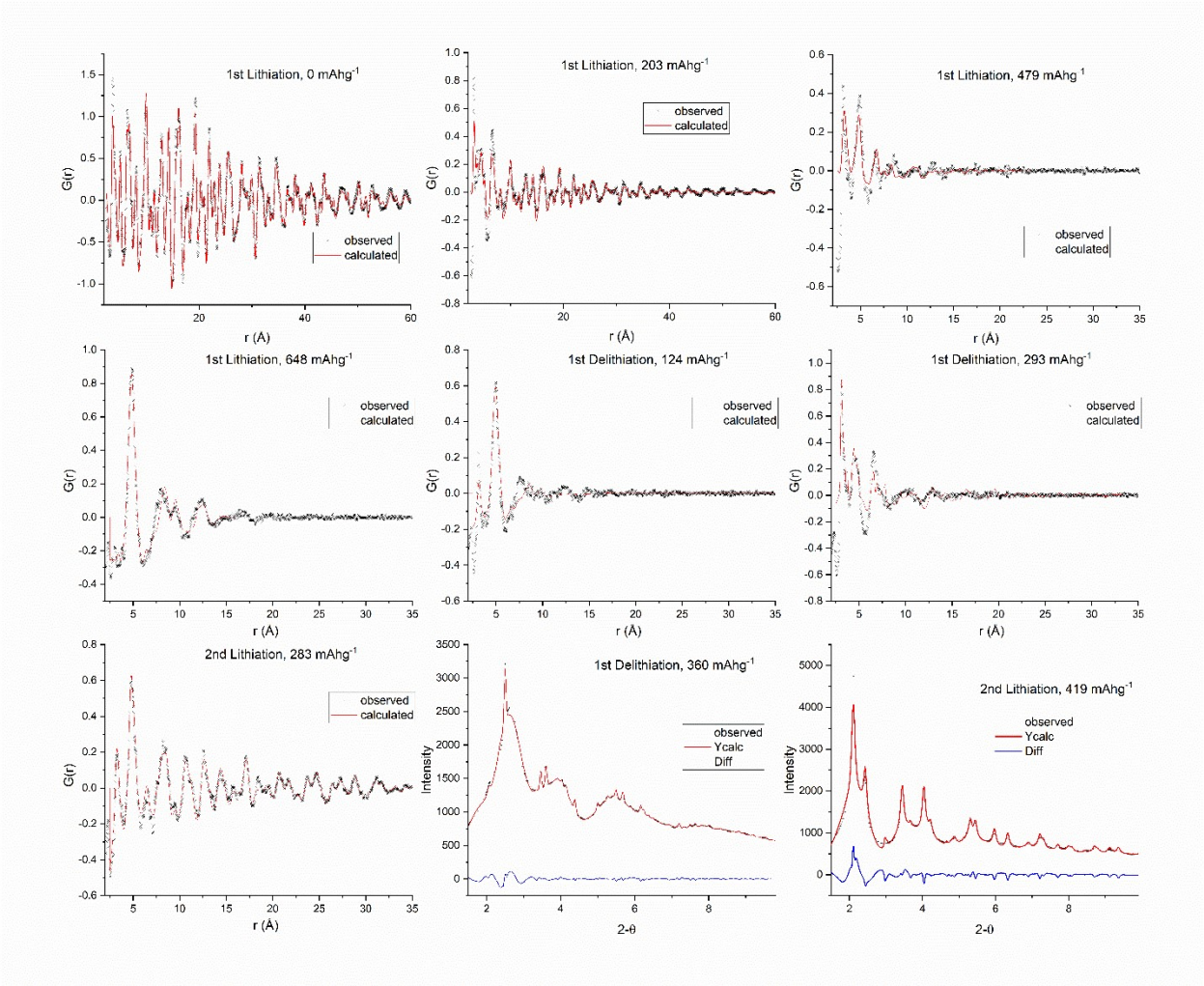

[Figure S6] example PDF and Rietveld fits at key points in the cycling process.

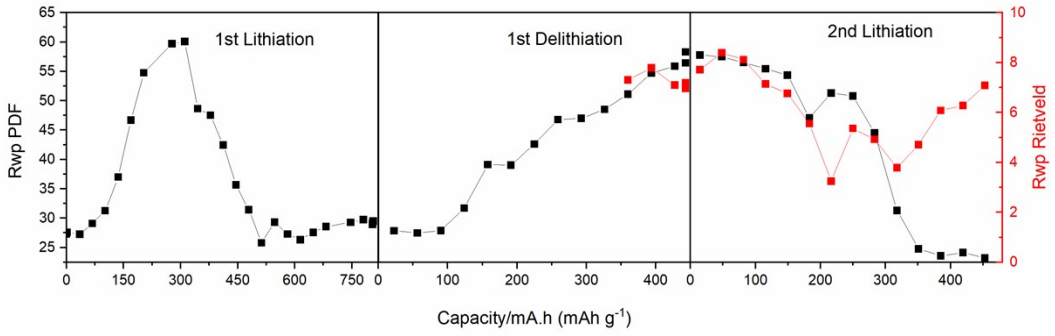

[Figure S7] Rwp values throughout the fitting process for PDF and Rietveld fits.

Anode coverage variations

The figure below is another illustration of the difference between XRD which is only sensitive to crystalline material and PDF which is also sensitive to the amorphous material. The difference image shows pixels where intensity is present in the PDF and not the XRD for the pristine $BiVO_4$ material before

cycling. Even for this very crystalline sample a clear that some areas are covered only by amorphous $BiVIO_4$.

The ensure that changes in anode coverage vs charge state in the TSCT maps were not influenced by beam intensity variations, the data were normalized to the intensity of the glass cell walls in each tomographic slice to give the data shown in the main manscript figures [pixel_counts] and [map_agglom].

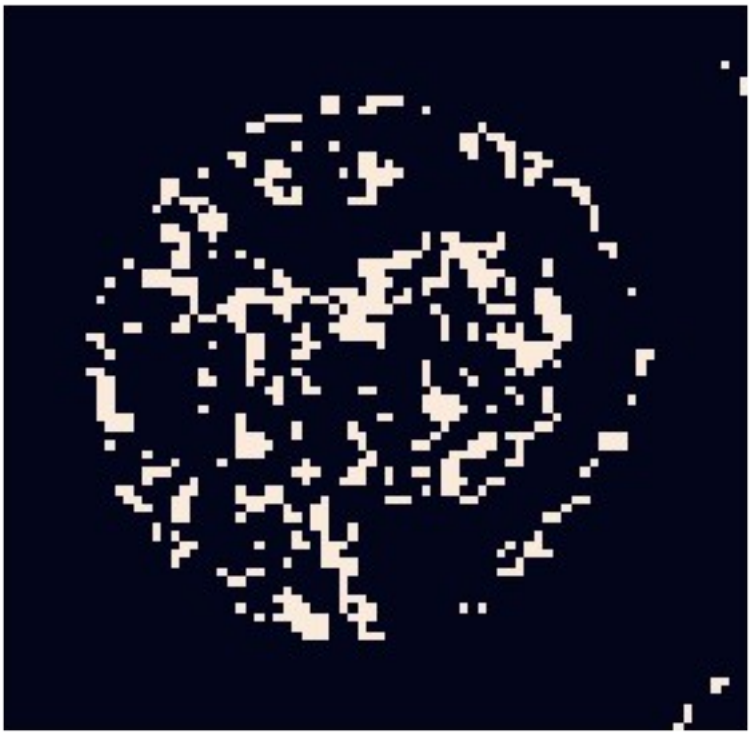

[Figure S8]- Difference plot of the coverage of anode material the cell at slice zero from XRD and PDFCT in slice zero for pristine $BiVO_4$ before lithiation. The coverage image was produced by marking all points above a threshold of 50% of the maximum intensity in the image as 1 and those below as 0. The XRD coverage image was then subtracted from the PDF one to produce the difference map. The positive difference indicates that more pixels are covered in the PDF coverage image.

The ensure that changes in anode coverage vs charge state in the TSCT maps were not influenced by beam intensity variations, the data were normalized to the intensity of the glass cell walls in each tomographic slice to give the data shown in the main manscript figures [pixel_counts] and [map_agglom].

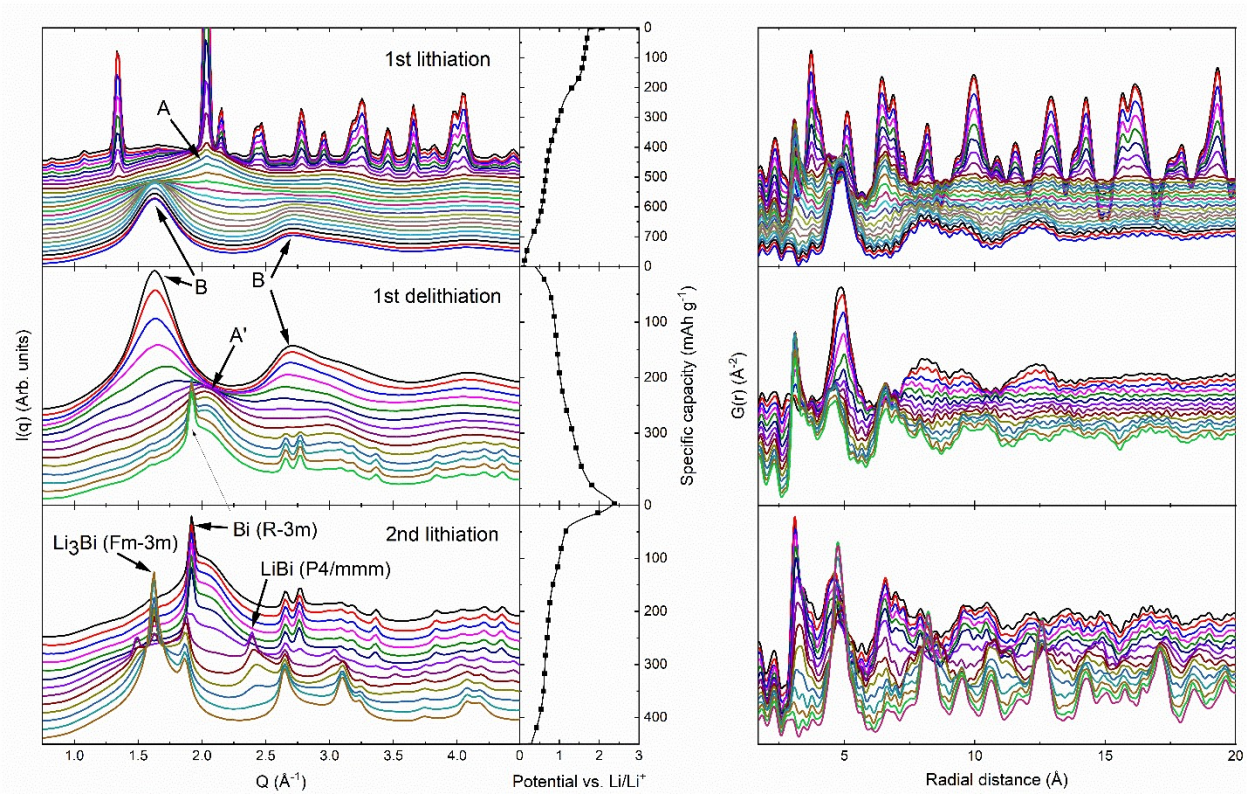

[Figure S9]- XRD and PDF data extracted from slice zero by summing the patterns from voxels covered by active material in the XRDCT plot of the pristine $BiVO_4$ before battery cycling was started. The peaks labelled (A) correspond to the diffraction signal of amorphous Bi. (B) peaks are from amorphous Li_3Bi and (A') is amorphous Bi in the first delithiation. The crystalline Li_xBi phases are labelled with their names and space groups.

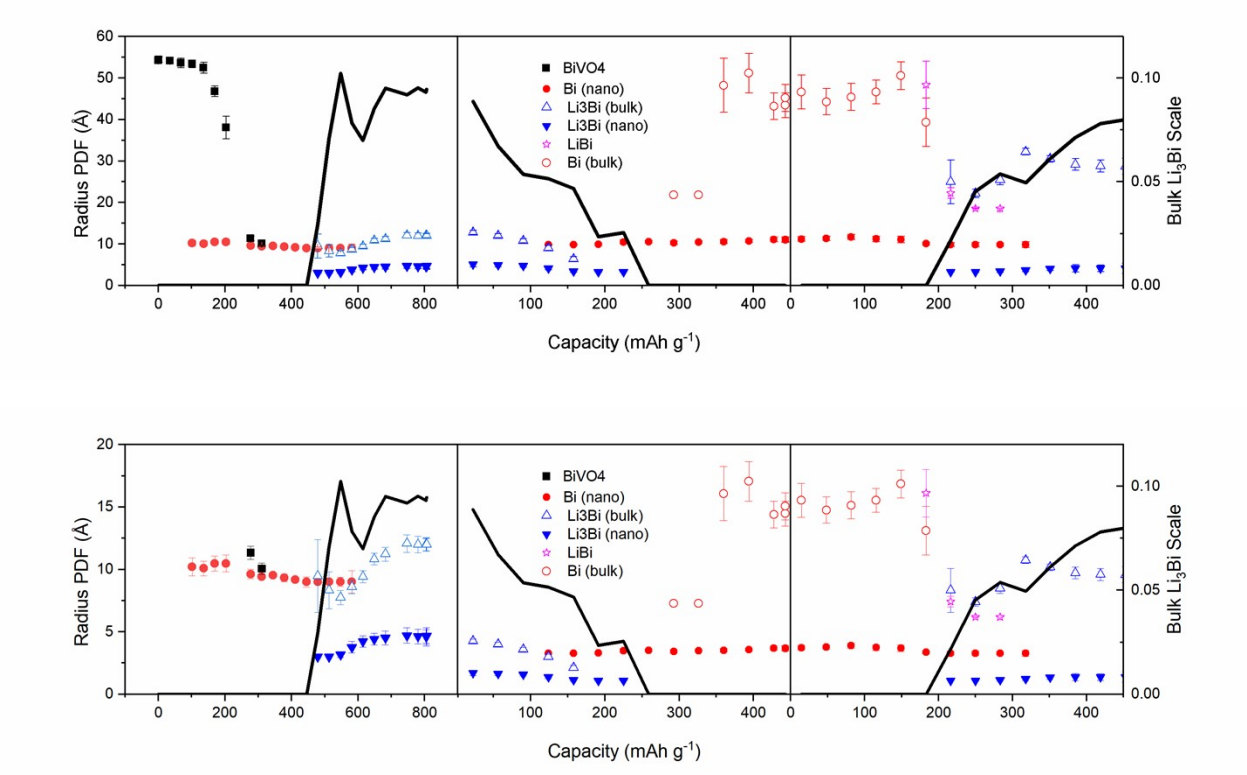

[Figure S10] variation of the radial damping parameters for the phases used in the PDF fits. The scale factor for the "bulk" Li_3Bi phase is plotted (solid black line) to indicate the progress of the reactions. The top version is scaled to show all data points including the highly crystalline pristine BiVO4, while the lower version uses a smaller scale to better illustrate the changes in PDF radius during cycling.

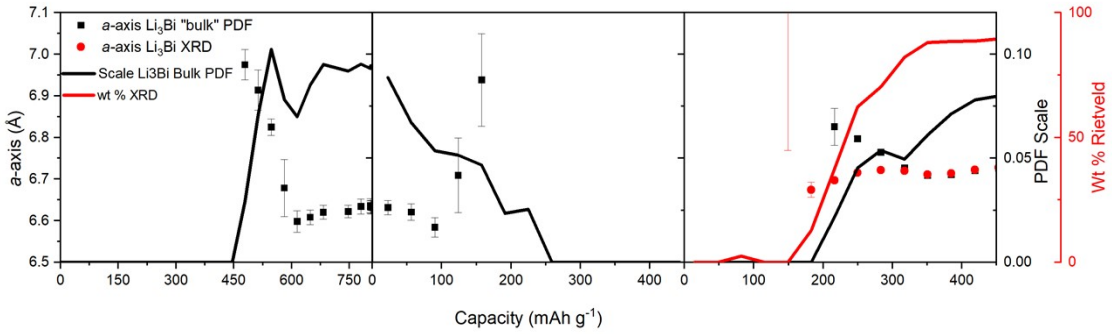

[Figure S11] Plot of the *a*-axis variation in the Li3Bi phase during the operando experiment. The scale factors (PDF and XRD) for the phase are shown so the axis length can be compared to the appearance and disappearance of the phase.

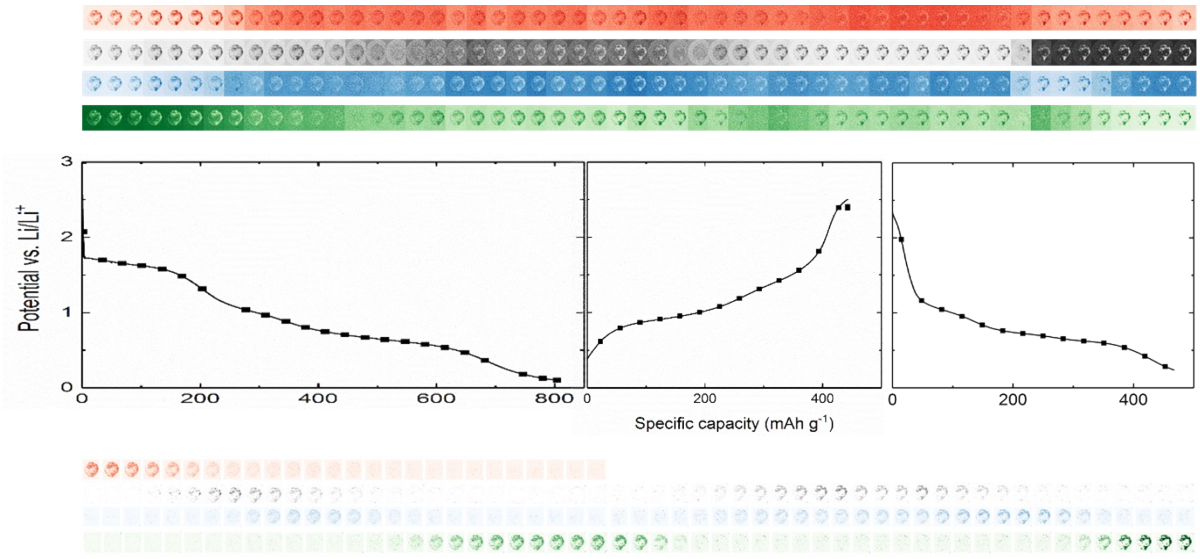

[Figure S12] Showing the XRDCT maps alongside the PDFCT maps shown in the main manuscript figure [PDFCT] reveals the total lack of clarity in the XRDCT maps (top) compared to PDFCT maps (bottom) for this process. This is mainly due to the absence of sharp Bragg peaks from the amorphous material formed in the first lithiation and still present at the start of delithiation.

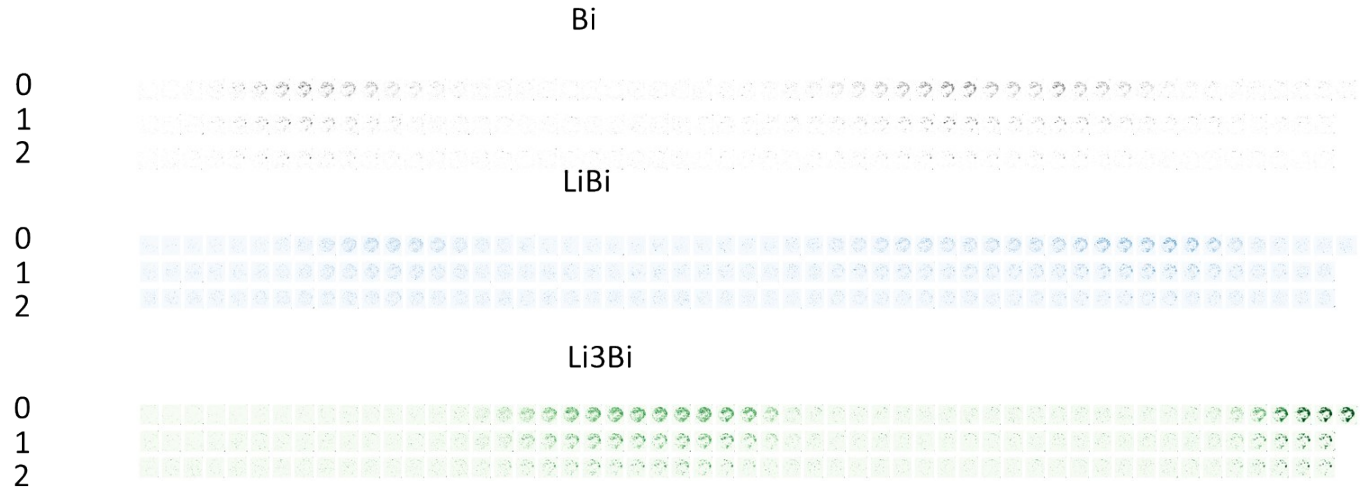

[Figure S13] PDFCT maps for the three LixBi phases showing axial variation in the amount of each phase visible (due to poor distribution of the active material painted onto the glassy carbon piston) but no differences in the time at which the phases appear/disappear in the 3 tomographic slices.

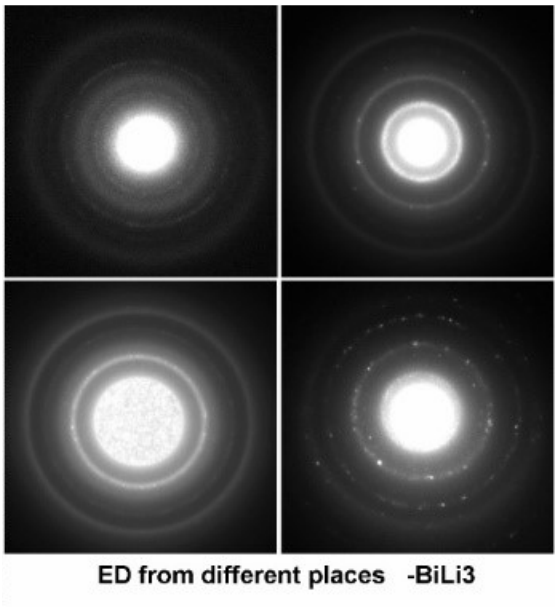

[Figure S14] Electron diffraction patterns identified as belonging to Li_3Bi, showing a mixture of powder and single crystal diffraction features from different parts of the sample, further indicating different levels of crystallinity.

DFT details

Total energies were calculated by the projected-augmented plane-wave (PAW) implementation of the Vienna *ab initio* simulation package (VASP).[4, 5] All these calculations were made with the Perdew, Burke, and Ernzerhof (PBE)[6] exchange correlation functional. Ground-state geometries were determined by minimizing stresses and Hellman-Feynman forces using the conjugate-gradient algorithm with force convergence less than 10^{-3}eV $Å^{-1}$. Brillouin zone integration was performed with a Gaussian broadening of 0.1 eV during all relaxations. From various sets of calculations it was found that 512 **k** points in the whole Brillouin zone for the structure with a 600 eV plane-wave cut-off are sufficient to ensure optimum accuracy in the computed results. The **k**-points were generated using the Monkhorst-Pack method[7] with a grid size of 8×8×8 for structural optimization. A similar density of **k**-points and energy cut-off were used to estimate total energy as a function of volume for all the structures considered for the present study. Iterative relaxation of atomic positions was stopped when the change in total energy between successive steps was less than 1meV/cell. All of the known stoichiometric crystal structures of

Li-P, Li-As, Li-Sb, Na-P, Na-As, Na-Sb, K-P, K-As and K-Sb were obtained from the International Crystallographic Structure Database (ICSD). For each structure the cations by Bi and all of the structures were then relaxed. The calculated total energy as function of all the phases considered in this study is given in figure S. A convex hull was generated between Li ($Im\bar{3}m$; 229)and Bi (R-3m; 166) see Figure [DFT].

For the electronic structure calculations of Li-V-O compounds the initial structures are collected from ICSD database and are relaxed to get the theoretical equilibrium.

Composition	cell volume/Å
$Li_{12}Bi_4$	304.67
$Li_{11}Bi_4$	302.70
$Li_{10}Bi_4$	293.12
Li_9Bi_4	282.27

[Table ST1] volumes of non stoichiometric $Li_{3-\delta}Bi$ compositions from DFT calculations

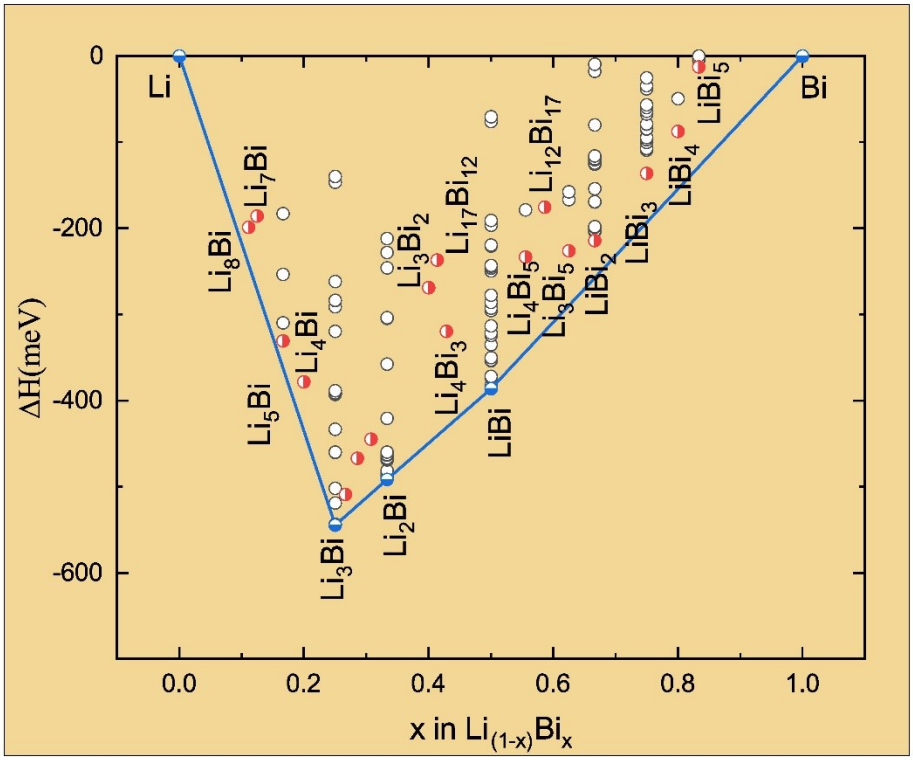

[Figure S15] The calculated convex hull diagram showing the lowest-energy phases in the Li–Bi phase diagram. The lowest energy route follows the blue line, with stable phases marked by

half-filled blue circles. The white circles are higher energy forms of the stable phases. The phases with higher energy than the convex hull are indicated by half-filled red circles.

Compound	Space group	Pearson symbol	Bandgap type	Bandgap (eV)
$Li_4V_3O_8$	*P*2_1/*m* (#11)	mP30	ID	0.695
LiV_2O_4	*Fd*-3*m* (#227)	cF56	HM	0
Li_3VO_4	*Pmn*2_1 (#31)	oP16	ID	4.01
Li_3VO_4	*Pnma* (#62)	oP32	ID	3.89
$LiVO_3$	*Cc* (#9)	mS40	ID	2.77
$LiVO_3$	*C*2/*c* (#15)	mS40	ID	3.03
$Li_2V_6O_{13}$	*C*2/*m* (#12)	mS42	HM	0
LiV_6O_{13}	*C*2/*m* (#12)	mS80	HM	0
LiV_2O_5	*Cmc*2_1 (#36)	oS32	ID	0.511
LiV_2O_5	*Pnma* (#62)	oP32	ID	0.829
LiV_2O_5	*Cmcm* (#63)	oS32	ID	0.261
LiV_2O_5	*Pmmn* (#59)	oP16	ID	0.354
$Li_3V_6O_{13}$	*C*2/*m* (#12)	mS44	HM	0
LiV_3O_8	*P*2_1/*m* (#11)	mP24	ID	1.75
$LiVO_2$	*R*3*m* (#166)	hR4	ID	1.34
$Li_2V_6O_{15}$	*C*2/*m* (#12)	mS46	HM	0

[Table ST2] Theoretically calculated (DFT) electronic structure information for Li-V-O compounds at the GGA level. bandgap types: ID- indirect; HM- semimetal

References

1. Ruud, A.; Sottmann, J.; Vajeeston, P.; Fjellvåg, H., Operando investigations of lithiation and delithiation processes in a BiVO4 anode material. *Physical Chemistry Chemical Physics* **2018,** *20* (47), 29798-29803.
2. Coelho, A., TOPAS and TOPAS-Academic: an optimization program integrating computer algebra and crystallographic objects written in C++. *Journal of Applied Crystallography* **2018,** *51* (1), 210-218.
3. Stinton, G. W.; Evans, J. S. O., Parametric Rietveld refinement. *Journal of Applied Crystallography* **2007,** *40* (1), 87-95.
4. Kresse, G.; Furthmüller, J., Efficient iterative schemes for ab initio total-energy calculations using a plane-wave basis set. *Physical Review B* **1996,** *54* (16), 11169-11186.
5. Kresse, G.; Furthmüller, J., Efficiency of ab-initio total energy calculations for metals and semiconductors using a plane-wave basis set. *Computational Materials Science* **1996,** *6* (1), 15-50.
6. Perdew, J. P.; Burke, K.; Ernzerhof, M., Generalized Gradient Approximation Made Simple. *Physical Review Letters* **1996,** *77* (18), 3865-3868.

7. Monkhorst, H. J.; Pack, J. D., Special points for Brillouin-zone integrations. *Physical Review B* **1976,** *13* (12), 5188-5192.